Research Article

Ines Nikolić, Jelena Antić-Stanković, Dragana Božić, Danijela Randjelovic, Bojan Marković, Dominique Jasmin Lunter, Aleksandar Kremenović, Miroslav Savić, and Snežena Savić*

Curcumin nanonization using an alternative small-scale production unit: selection of proper stabilizer applying basic physicochemical consideration and biological activity assessment of nanocrystals

https://doi.org/10.1515/rams-2020-0043
Received Jan 31, 2020; accepted Jul 17, 2020

Abstract: As the number of poorly soluble drugs is increasing, nanocrystals have become very interesting due to wide range of application possibilities. Curcumin was used as a model active ingredient in this work. Even though it has many proven positive effects, due to its physicochemical issues, its possibilities have not been fully exploited.
The goal of this work was to select optimal conditions for a top-down method for curcumin nanosuspension production, and to perform their comprehensive characterization applying complementary methodologies: dynamic light scattering, polarization and atomic force microscopy, thermal analysis, X-ray powder diffraction, antioxidant activity evaluation, release kinetics assessment, and screening of potential biological effects applying cell viability assays on normal human lung fibroblasts, human melanoma and human adenomacarcinoma cells.
After 30 min of milling, nanosuspensions stabilized by polysorbate 80 and by its combinations with sucrose palmitate showed good stability, while curcumin crystal structure was unaltered. Obtained nanocrystals were well defined, with average diameter 120–170 nm and PDI of about 0.25, zeta potential was below –30 mV and pH~5 for all formulations. Nanodispersions exhibited high antioxidant potential and improved dissolution rate compared to the corresponding coarse dispersions. Although curcumin nanodispersions exhibited significant antiproliferative effect to each cancer cell line, the highest effect was towards adenocarcinoma cells.

Keywords: nanocrystal; curcumin; top-down method, wet-ball milling

***Corresponding Author: Snežena Savić:** Department of Pharmaceutical Technology and Cosmetology, University of Belgrade – Faculty of Pharmacy, 11000 Belgrade, Serbia;
Email: snezana.savic@pharmacy.bg.ac.rs; Tel.: +381-11-3951288; Fax: +381-11-3972840
Ines Nikolić: Department of Pharmaceutical Technology and Cosmetology, University of Belgrade – Faculty of Pharmacy, 11000 Belgrade, Serbia
Jelena Antić-Stanković, Dragana Božić: Department of Microbiology and Immunology, University of Belgrade – Faculty of Pharmacy, 11000 Belgrade, Serbia
Danijela Randjelovic: Institute of Chemistry, Technology and Metallurgy, Department of Microelectronic Technologies, University of Belgrade, 11000 Belgrade, Serbia
Bojan Marković: Department of Pharmaceutical Chemistry, University of Belgrade – Faculty of Pharmacy, 11000 Belgrade, Serbia
Dominique Jasmin Lunter: Institute of Pharmaceutical Technology, Eberhard-Karls University, D-72076 Tübingen, Germany
Aleksandar Kremenović: Laboratory of Crystallography, Faculty of Mining and Geology, University of Belgrade, 11000 Belgrade, Serbia
Miroslav Savić: Department of Pharmacology, University of Belgrade – Faculty of Pharmacy, 11000 Belgrade, Serbia

1 Introduction

Nowadays, the majority of newly discovered active pharmaceutical ingredients are extremely poorly soluble. Such characteristic results in low bioavailability and obstacles in reaching the anticipated action site, hindering their performances *in vivo*. Poorly soluble drugs can be characterized either as *grease balls* or *brick dust* molecules [1]. In spite of low water solubility, *grease balls* have a certain oil solubility, which enables them to be incorporated in a lipid-based formulation. On the other hand, *brick dust* molecules are poorly soluble both in oils and in polar solvents, which represents a difficulty in their application. However, there are several strategies that can be ap-

plied in order to overcome the problematic physicochemical properties of active molecules [2, 3]. Based on evidence and accumulated knowledge, it has been established that nanotechnology can enable a therapeutic platform for improved drug delivery [4–9]. These expectations could be achieved through the specific properties of nanomaterials, such as size, shape and surface functionalities [10]. Alongside nanostructured drug delivery systems, which enable drug solubilization, protection, controlled release and targeting, nanosuspensions, also referred as *carrier free* formulations [3], represent a promising option for extremely poorly soluble molecules through improvement of their bioavailability [11].

Analyzing development of nanomaterials for drug delivery, we are witnessing the emergence of a range of different nanosystems. According to the statistics from 2018, nanosystems have most commonly been used as carriers for drugs intended for cancer, inflammatory and immunological diseases - more than 50% of the total number of approved nanomedicines by the US Food and Drug Administration. Among them, liposomes are in the first place, followed by nanocrystals and nanoemulsions [12–16].

Drug nanocrystals can be defined as submicron crystalline particles of the drug (100-1000 nm), with average diameter usually below 500 nm. They are stabilized by surfactant, a polymer stabilizer, or their combination [3]. Due to such a small size, some intrinsic properties of a molecule change dramatically. For example, solubility, dissolution rate and adhesiveness to the biological membranes are much higher compared to a standard, "macro" crystal, enabling some specific advantages that can be achieved *in vivo*. They increase drug bioavailability, consequently boosting the effectiveness, which is especially useful for poorly soluble active molecules [2, 3, 17, 18].

Drug nanocrystals are commonly formulated as aqueous nanosuspensions, but with some further processing steps, they can also be transformed to other dosage forms, suitable for various administration routs (dermal, parenteral, ocular...). As very low concentration of surfactant is applied for nanosuspension formulation, their safety profile is very favorable [19].

Regarding nanocrystal production, there are 2 possible approaches: *top-down* and *bottom-up*. *Top-down* methods are based on lowering the size of the bulk material (containing bigger particles) through milling procedures, whereas *bottom-up* rely on the opposite mechanism – they start from a dissolved drug, and nanocrystals are obtained upon precipitation. Owing to more reliable process control and easier *scale up*, *top down* processes are preferable. Due to small size, and corresponding large specific surface, nanosuspensions are prone to physical destabilization processes (kinetic instability) during storage, so not only their production, but also stabilization acts as a challenge [18].

During the recent years, there has been an evident trend of return to the natural sources of medicinal compounds. With this regard, curcumin, a polyphenol extracted from the rhizome of the *Curcuma spp*. (*Zingiberaceae*) represents a phytochemical compelling for therapeutic use due to its numerous beneficial properties for human health. Its antioxidant and anti-inflammatory activities are underlined, and anticancer potential is frequently discussed in the literature [20, 21]. Even though this pleiotropic potential has been well established, curcumin's *in vivo* performances are hindered due to low solubility, physicochemical instability, rapid metabolism, and poor penetration and targeting efficacy. Being a representative of a demanding active molecule, curcumin is regarded as an excellent candidate for application in the form of nanocrystals.

Therefore, the main goal of this work was to select appropriate process and formulation parameters for a *top-down* method for curcumin nanocrystal preparation, and to conduct a comprehensive physicochemical characterization of selected dispersions, with reference to potential dermal application. Further on, the idea was to assess the *in vitro* antioxidant potential, as well as safety profile and effectiveness of developed dispersions in biological assays using 3 cell lines: normal human lung fibroblasts, human malignant melanoma and human cervical adenocarcinoma. The principal idea was to provide sufficient data on curcumin nanocrystal performances that could pave a road to some further development and application.

2 Materials and methods

2.1 Materials

For nanosuspension preparation, the following components were used: curcumin (Sigma–Aldrich Co; St. Louis, USA), polysorbate 80 - P80 (Acros Organic, Thermo Fisher Scientific Company; Geel, Belgium), sucrose palmitate – SP (Mitsubishi–Kagaku Foods Corporation; Tokyo, Japan), methylcellulose – MC (Sigma–Aldrich Co; St. Louis, USA), and ultra-purified water – W, provided by the Gen Pure apparatus (TKA Wasseranfbereitungs system GmbH, Neiderelbert, Germany). All other chemical used in the experiment were of HPLC grade.

2.2 Methods

2.2.1 Sample preparation

For sample preparation, a procedure mimicking wet ball milling was performed. Similar process has already been reported by Corrias *et al.* [22]. Briefly, coarse dispersions of curcumin were prepared using a rotor-stator homogenizer (UltraTurax, IKA, Staufen, Germany), and further nanonization was conducted in a Cell Disruptor Genie (Scientific Industries, USA), applying yttrium stabilized zirconium dioxide beads (Sigmund Lindner, Warmensteinach, Germany; diameter 0.1-0.2 mm) as the milling medium. Firstly, the stabilizer solution was prepared in ultra-purified water, and then curcumin was added, which was followed by 3-minute homogenization (8000 rpm). After the coarse dispersion had been prepared, a defined volume was transferred to 2 ml tubes prefilled with zirconium dioxide beads (60% *v/v*). Nanonization was carried out at 3000 rpm, checking selected properties of the particles at predefined time points: after 10, 30 and 60 minutes of milling. The concentration of curcumin was fixed to 1 mg/ml, and the effect of three different stabilizers (solely and in combinations) on the milling procedure and stability of obtained dispersions was evaluated.

2.2.2 Particle size assessment

In order to measure the size of the dispersed phase, photon correlation spectroscopy was performed using *Zetasizer Nano ZS90* (Malvern Instruments Ltd, Worcester, Malvern, UK). As sizing parameters, intensity weighted mean diameter (Z-average diameter, Z-ave) and polydispersity index (PDI) were determined. Prior to measurements, samples were diluted with ultrapure water (1:100, *v/v*) in order to obtain optimal scattering intensity.

2.2.3 Zeta potential measurements

Zeta potential (ZP), as a measure of particle surface charge and one of the long-term stability indicators, was determined through measurements of electrophoretic mobility of nanoemulsion droplets, using Zetasizer Nano ZS90 (Malvern Instruments Ltd., Worcester, Worcestershire, UK). The measurements were conducted immediately upon diluting the samples (1:100, *v/v*) with ultrapure water, at 25°C, with conductivity adjusted to 50 μS/cm using 0.9% (*w/v*) sodium chloride solution.

2.2.4 pH measurements

As an important parameter for curcumin's stability, pH of selected samples was also determined (Hanna Instruments Inc, Michigan, USA) at 25°C.

2.2.5 Polarization microscopy

In order to get an insight into the size and morphology of the curcumin crystals before and after nanonization, polarization microscopy was performed using *Carl Zeiss Apo-Tome Imager Z*1 microscope (Zeiss, Göttingen, Germany), integrated with the AxioCam ICc1 camera.

2.2.6 Thermal analysis

To check the crystalline state of the curcumin powder, and to verify that crystalline state was not changed after the nanonization, differential scanning calorimetry (DSC) was conducted by Mettler DSC 820 apparatus (Mettler Toledo GmbH Analytical, Giessen, Germany). Air-dried samples were placed in standard aluminum pans, hermetically sealed and subjected to the heating program from 25°C to 200°C with the heating rate of 2 K/min, under constant nitrogen flow. An empty aluminum pan served as a reference.

2.2.7 Atomic force microscopy

For direct observation of the obtained nanocrystals and morphological evaluation, atomic force microscopy was performed applying AutoProbe CP-Research SPM (TM Microscopes-Bruker, Germany). 10 μl of each sample was directly placed on the circular mica substrate (Highest Grade V1 AFM Mica Discs, Ted Pella Inc., Redding, California, USA) and dried in vacuum. AFM measurements were performed in air, using noncontact probes Bruker Phosphorous (n) doped silicon Tap300, model MPP-11123-10 with Al reflective coating and symmetric tip. Driving frequency of the cantilever was about 300 kHz. Topography and "error signal" images were captured and analyzed.

2.2.8 X-Ray Powder Diffraction analysis

Selected samples of nanodispersions, as well as their stabilizers, were investigated by the X-Ray Powder Diffraction (XRPD). Measurements were conducted on Rigaku Smart-

lab X-ray Diffractometer in θ-θ geometry (the sample in horizontal position) in parafocusing Bragg-Brentano geometry using D/teX Ultra 250 strip detector in 1D standard mode with CuK$\alpha_{1,2}$ radiation source (U = 40 kV and I = 30 mA). The XRPD patterns were collected in 3-40° 2θ range, with step of 0.01°, and data collection speed of 3°/min. The low background single crystal silicon sample holder was used to minimize the background. Unit cell parameters as well as average crystallite size and strain values for curcumin are obtained through Whole Powder Patter Fitting (WPPF) procedure incorporated in PDXL2 integrated X-ray powder diffraction software (Version 2.8.30; Rigaku Corporation).

2.2.9 In vitro release/dissolution study using Franz diffusion cells

In order to be easier for application, selected nanosuspensions and corresponding coarse suspensions were thickened by xantan (1%). The study was performed using *Franz* diffusion cells (*Gauer Glas*, *D-Püttlingen*, Germany). In each cell, 1g of the formulation was deposited. The study was performed in triplicate, applying the protocol described by Nikolic *et al.* [23]. More details are provided in the *Supplementary material section*.

2.2.10 Evaluation of the antioxidant activity of the nanocrystal dispersions

For the purpose of antioxidant evaluation, a spectrophotometric free radical scavenging assay - DPPH (2, 2-diphenyl-1- picrylhydrazyl) was performed. Briefly, in glass cuvettes, 3.6 ml of DPPH solution in methanol (0.1 mM) was mixed with 400 µL of the test sample with curcumin. Nanocrystal dispersions were diluted in ultrapure water in order to obtain the following curcumin concentrations: 0.25, 0.1875, 0.125, 0.0625, and 0.03125 mg/ml. In this manner, the absorbance values in the range 0.2-0.8 were covered. After 30 minutes of incubation at room temperature, in dark and under constant shaking (350 rpm), the absorbance of the samples was recorded at 517 nm, using a spectrophotometer (Varian Cary-100 UV–VIS Varian BV, Middelburg, Netherlands). The blank sample was prepared with 400 µL of the corresponding stabilizer solution. The percentage of inhibition was calculated using the following equation:

$$I = [(Ac - As)/Ac] \times 100; \quad (1)$$

where I stands for inhibition percentage, A_c for absorbance of a blank sample, and A_s for absorbance of the test sample. The inhibition percentage was plotted against concentration of the samples, and IC_{50} values, as the mean value of three measurements, was determined by linear regression analysis. Activity of bulk curcumin was estimated in the similar manner, following the protocol described by Nikolic *et al.* (2018).

2.2.11 LC-MS/MS analysis

Determination of curcumin content during the release/dissolution study was performed by liquid chromatography coupled with mass spectrometry (LC-MS/MS) technique. For detail on the analytical procedure, please consult the *Supplementary material* section.

2.2.12 Biological activity evaluation

Cell lines

For this experimental section, three cell lines were used: human cervical adenocarcinoma (HeLa), human malignant melanoma (Fem-x), and normal, human lung fibroblast (MRC-5), obtained from American Type Culture Collection (Manassas, VA, USA). Cells were maintained in complete nutrient medium RPMI-1640 (Sigma-Aldrich, St. Louis, USA), at 37°C and in humidified atmosphere with 5% CO_2. The nutrient medium was supplemented to with L-glutamine (3 mM), streptomycin (100 mg/mL), penicillin (100 IU/mL), and fetal bovine serum (10%; heat-inactivated at 56°C for inactivation of cholinesterases, system complement and HEPES (25 mM)). Bicarbonate solution was used for pH adjustment to 7.2.

Preparation of stock solutions

Firstly, solution of curcumin was prepared in dimethyl sulfoxide (DMSO) and then diluted in the cell medium, so that the final DMSO concentration was below 0.1%, and curcumin concentration was set to the 600 µg/ml. Nanocrystal dispersions were also diluted in the cell medium giving the same concentrations. The blank samples (surfactant solution in ultra-pure water) were diluted in the same manner as the curcumin dispersions. All samples were afterwards mixed with the nutrient medium, providing relevant working concentrations.

Treatment of the cell lines

The HeLa (2×10^3 cells per well), Fem-X (5×10^3 cells per well) and MRC-5 (5×10^3 cells per well) cells were seeded

into 96-well microtiter plates, and 24 h later, after cell adherence, five different concentrations of the test samples were added to the wells. The final test concentrations of curcumin ranged from the 12.5 μg/ml to 200 μg/ml. Corresponding dilutions of the blank formulation were also investigated. In the control wells, only nutrient medium was added to the cells.

Determination of target-cell survival

Cell survival was determined 48h after the addition of the test samples, conducting the MTT test, (3-(4,5-dimethylthiazol-2-yl)-2,5-diphenyl tetrazolium bromide – MTT; Sigma-Aldrich, St. Louis, USA). MTT was dissolved in phosphate buffered saline (PBS) pH 7, in the concentration 5 mg/mL, and filtered through Millipore filters (0.22 μm) prior to use.

Firstly, 10 μL of the MTT solution was added to each well. The samples were incubated for additional 4 h at 37°C, with 5% CO_2 and humidified atmosphere. Then, 100 μL of the 10% solution of sodium dodecylsulfate – SDS (Sigma-Aldrich,St. Louis, USA) was added to each of the wells. The next day, absorbance of the cell medium from each well was measured at 570 nm, using Multiskan™ FC Microplate Photometer (Thermo Scientific, USA) and cell survival (%) was calculated.

The concentration that decreased treated cell survival by 50% (IC50) was determined from the graph, by numerical analysis of the obtained data. Selectivity index was calculated by dividing the IC50 value for MRC-5 with IC50 value for Fem-X or HeLa, for each investigated sample.

Three independent experiments were made, each was performed in triplicate, and results were presented as mean values ± SD.

2.2.13 Statistical analysis

Physicochemical measurements were performed in triplicates, and results were presented as the mean value of the observed parameter ± standard deviation. For statistical significances assessment, Student t-test was performed, and statistical significance was set at $p<0.05$.

3 Results and discussion

3.1 Selection of the stabilizers and optimization of the milling time

In order to provide optimal stabilization of the curcumin nanosuspension, 3 different stabilizers were evaluated (polysorbate 80 - P80; sucrose palmitate – SP; methyl cellulose - MC). They were selected as they represent different stabilizer types: MC is a polymeric molecule, P80 is a well-established surfactant, and SP is relatively new and biodegradable surfactant derived from natural sources [24]. Several stabilizer concentrations were tested, as well as some of their mutual combinations, with a view to obtain the optimal ratio. Firstly, formulations only with one stabilizer were prepared. Afterwards, in order to reduce the concentration of the ethoxylated surfactant, two combinations of P80 and SP were also tested (P80:SP=4:1 and P80:SP=2:1). Curcumin concentration was fixed to 1 mg/ml, and the ratio curcumin:stabilizer warried as followed: 1:1; 1:2.5 and 1:5.

Prior to the nanonization process, the coarse dispersions were observed under the polarization light in order to analyze the features of the curcumin crystals. Dispersed particles were of irregular shape (isometric and elongated rod-like) and their size was in the micrometer range, with broad size distribution (Figure 1).

After the milling procedure had been performed, dispersions were packed in glass vials, sealed and monitored for any curcumin precipitation for 24 h at room temperature. To select the optimal milling time, the milling process was performed for 10, 30 and 60 minutes, and obtained results in terms of size and size distribution were compared. For the most promising formulations, the ones that did not exhibit any precipitation (Table 1, Table 2), size and size distribution were determined, and their stability was further followed.

As presented in the Figure 2, there is an expected trend of the particle size decrease that follows longer milling time. Contrastingly, when it comes to the PDI, a different pattern can be noticed – if the milling procedure lasts more than 30 minutes, PDI increases as well. Similar findings were reported by Kakran *et al.* [25]. Such result probably emanates from the "over processing" phenomenon. Briefly, during the nanonization, crystals firstly break at the points called *crystal imperfections*, where the crystalline structure is the most fragile. As the process goes further, these areas become less present, and the crystals become more perfect. Consequently, the force required for crystal breakage is higher. Increase in energy input leads to the size re-

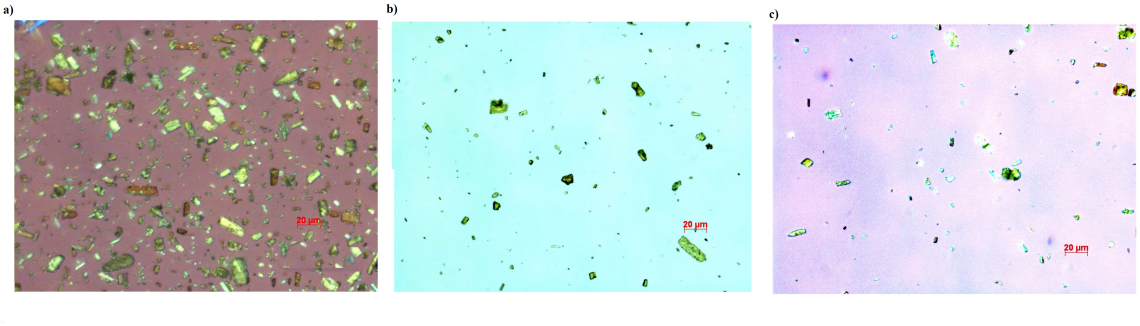

Figure 1: Polarization microscopy images of the coarse dispersions of curcumin: a) F_P80; b) F_P80/SP_4:1; F_P80/SP_2:1

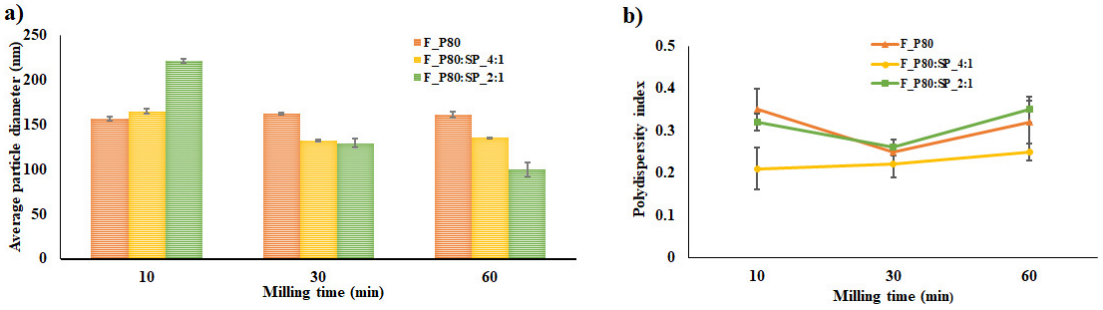

Figure 2: Average particle diameter (a) and polydispersity index (b) of the curcumin dispersions obtained after 10, 30 and 60 minutes of milling

Table 1: Screening of potential stabilizers and their concentrations for nanosuspension preparation

Stabilizer	Stabilizer:CU ratio			CU concentration
P80	1:1	1:2.5	1:5	1 mg/ml
Precipitation within 24 h	**No**	Yes	Yes	
SP	1:1	1:2.5	1:5	1 mg/ml
Precipitation within 24 h	Yes	Yes	Yes	
MC	1:1	1:2.5	1:5	1 mg/ml
Precipitation within 24 h	Yes	Yes	Yes	
P80/SP=4:1	1:1	1:2.5	1:5	1 mg/ml
Precipitation within 24 h	**No**	Yes	Yes	
P80/SP=2:1	1:1	1:2.5	1:5	1 mg/ml
Precipitation within 24 h	**No**	Yes	Yes	

P80 - polysorbate 80; SP – sucrose palmitate; MC – methyl cellulose; CU - curcumin

Table 2: Qualitative and quantitative (%) composition of selected nanosuspensions

Formulation name	P80	SP	CU	W
F_P80	0.1	/	0.1	99.8
F_P80/SP_4:1	0.08	0.02	0.1	99.8
F_P80/SP_2:1	0.067	0.033	0.1	99.8

P80 - polysorbate 80; SP – sucrose palmitate; MC – methyl cellulose; CU - curcumin

duction up to a certain point, providing more energy to break the crystals into smaller ones, and giving enough time to the stabilizers to attach to the newly formed surface [26]. However, at some point, when the disruption force becomes equal to the attraction forces of the crystalline structure, no further size reduction is possible at given nanonization conditions [27]. As energy continues to be delivered to the system, the kinetic energy of the crystals becomes higher, causing aggregation [25]. Similar findings were observed by Rachmawati *et al.* [28] and Hu *et al.* [26] for 2 different methods – high pressure homogenization and wet media milling. Such event is unfavorable with regard to the long-term stability because the particles may exceed the energy barrier according to the DLVO theory, and undergo coalescence [29].

It is important to mention that different stabilizers have distinct effect on the physicochemical stability of the nanocrystal dispersions, both during shelf-life and when exposed to the physiological conditions [28, 30]. Not only the presence of microparticles should be the lowest possible, but also the size distribution of the dispersed particles should be homogeneous, regardless the exact value of the mean particle diameter. This is crucial both for stability of the dispersion and imposed bioavailability expectations [29, 31]. Hence, in the presented experimental setting, nanonization time of 30 minutes was found as the optimal one.

3.2 Determination of pH and zeta potential

In order to maintain the chemical stability of curcumin in the formulation, it is of high importance to have a pH in the acidic region, as it is well known that curcumin undergoes oxidative degradation in the alkaline conditions. All three selected formulations had pH around 5 (Table 3), proving the appropriate conditions. Moreover, as a hint of physical stability of the dispersion, zeta potential was measured. Even though these formulations are stabilized by nonionic surfactants, providing steric stabilization, obtained zeta potential values were quite high (Table 3). Values below −30 mV generally suggest very good physical stability [32], preventing aggregation and cake formation. In this case, as nonionic stabilizers were used, obtained values may be due to pH of the dispersions. Namely, curcumin is prone to keto-enolic tautomerization, and in the acidic environment, diketo form prevails, being a potent proton-donor [21]. Accordingly, it may influence the surface electrical properties.

Table 3: Determined pH and zeta potential values of the selected formulations

Formulation	pH	Zeta potential (mV)
F_P80	5.3 ± 0.1	−30.5 ± 4.9
F_P80/SO_4:1	5.20 ± 0.05	−33.4 ± 3.5
F_P80/SO_2:1	4.9 ± 0.1	−35.1 ± 2.9

3.3 Atomic force microscopy, thermal analysis and X-ray powder diffraction

To directly observe obtained curcumin nanocrystals, atomic force microscopy was performed. It enabled 3D analysis of the particles, their size and morphology. Sigle particles as well as the profile of selected ones are depicted in the Figure 3. It was noted that, after the nanonization, particles became more homogeneous in size and shape. However, slight disagreement of the estimated size obtained after DLS may be attributed to the sample preparation, and nonspherical shape of the crystals (contrastingly the assumption supporting DLS size estimation) [33].

In addition, it is well known that some stress conditions (such as milling or exposure to different temperature conditions) can influence the physical state of the compound, inducing some amorphisation [34]. Such event, in terms of nanocrystal formulations, may be an undesired consequence. Therefore, the crystallinity of curcumin dispersion was checked before and after the nanonization with a view to check the physical state and structural organization of the material, applying DSC measurements and XRPD.

Bulk material (curcumin before nanonization) exhibited a sharp endothermic peak at 174°C (Figure 4), which corresponds to its melting temperature. After the milling, formulations were subjected to the same analysis. Due to the possibility of the water evaporation peak to overlap the curcumin's melting peak, prior to the analysis, water was removed from the samples using a vacuum pump. Again, there was a visible endothermic peak corresponding to the melting of the curcumin's crystalline structure, pointing out that no amorphisation occurred. However, it was visible that the melting temperatures were shifted towards lower values. Such finding confirmed that at the nanoscale, some fundamental physicochemical features of a molecule change (*e.g.* melting point and solubility). Assuming spherical shape of a nanocrystal, a linear relationship has been found between the melting point and a reciprocal value of the particle size, underlining that melting point decreases with decrease in the particle size [35].

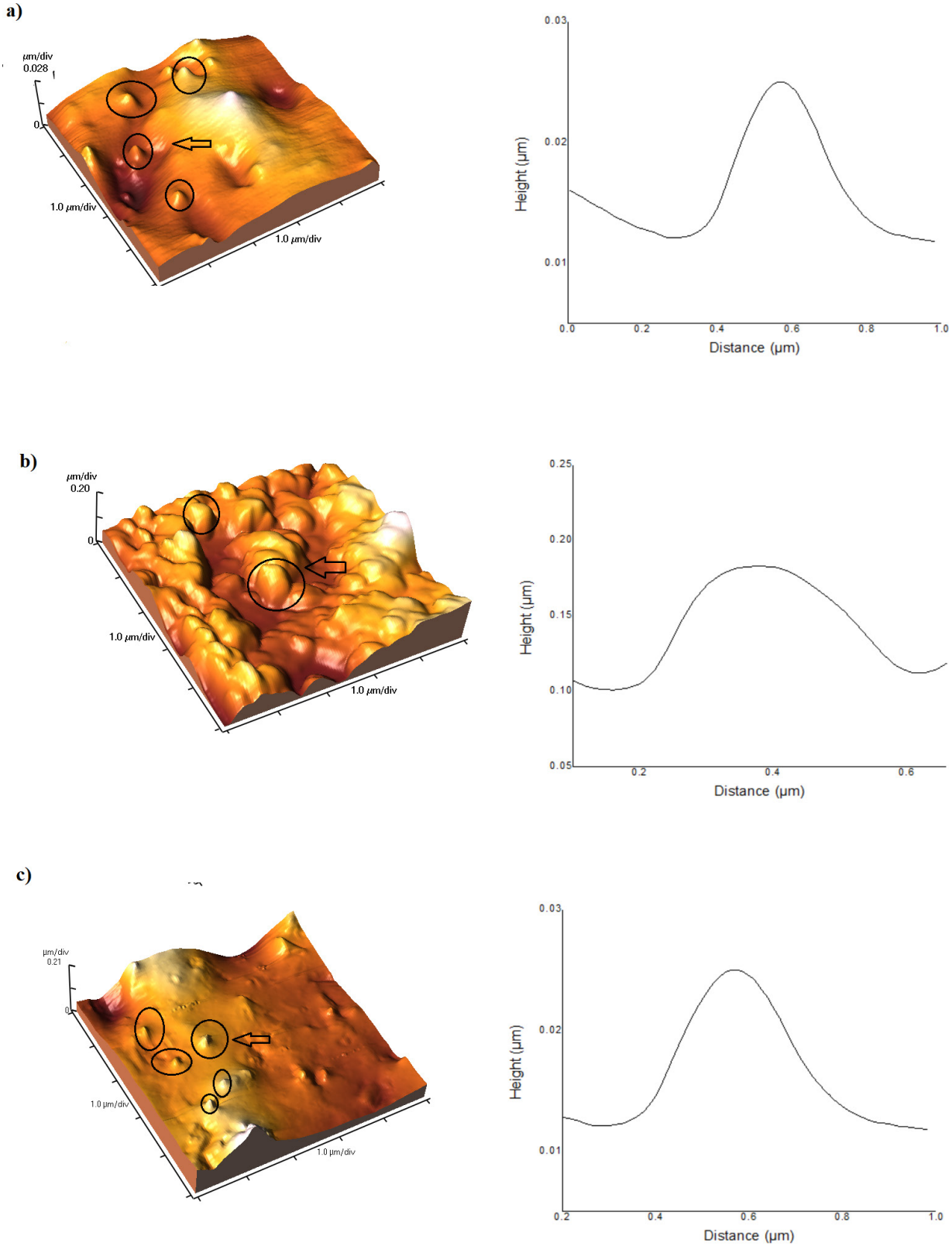

Figure 3: 3D atomic force microscopy images of the investigated curcumin nanocrystal dispersions and corresponding height-distance profiles for selected particles (marked with an arrow): a) F_P80; b) F_P80/SP_2:1; c) and d) F_P80/SP_4:1

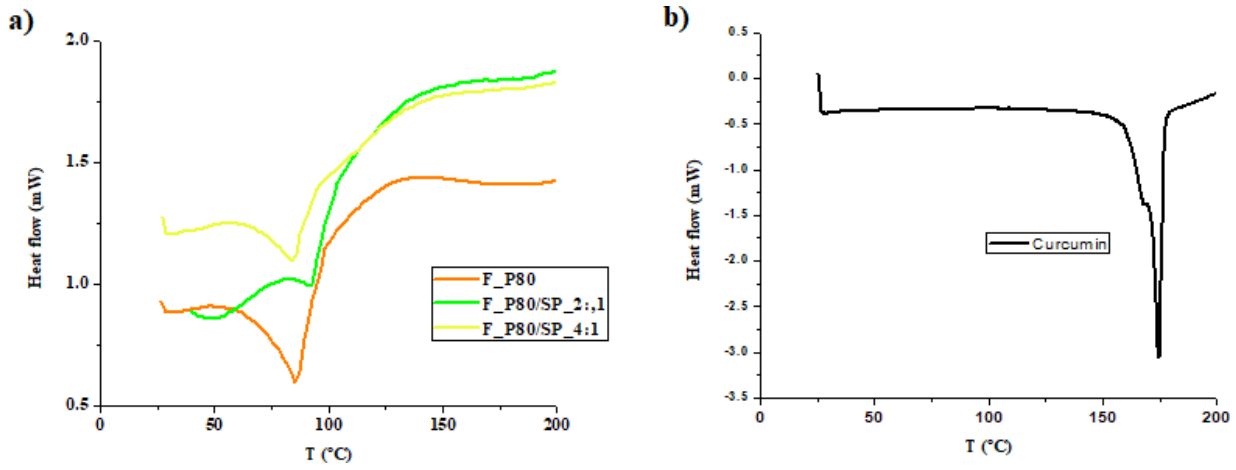

Figure 4: Differential scanning calorimetry thermograms of the curcumin nanocrystal dispersions (a) and bulk curcumin (b)

$$T_m(D) = T_{m0}\left(1 - \frac{\beta}{D}\right) \quad (2)$$

where D is the particle diameter, T_m and T_{mo} are melting temperatures of a nanocrystal and bulk material, respectively, and β a material constant.

Further on, in some succeeding works, it has been established that not only size, but also shape has influence on the melting properties of material [36, 37]. Lu *et al.* [36] developed a model for prediction of size, shape and dimensionality effect on the melting point of nanocrystals:

$$\frac{T_m(D,\ d,\ \lambda)}{T_{m0}} \approx \frac{(3-d)\,hS_{b0}\lambda}{9RD} \quad (3)$$

where D denotes the diameter, d a dimensionality parameter (for spherical particles d=0, for cylindrical nanowire d=1, for thin films d=2), λ a shape parameter (varying from 0 to 3, for spherical particles, cubic particles, cubic and cylindrical nanowires and thin films λ=1), R is ideal gas constant, S_{bo} is the bulk solid-vapor transition entropy, and h denotes atomic diameter.

Hence, the melting temperature of a crystal decreases with increasing λ or decreasing D and d.

Some authors hypothesized that shift in the melting point with significantly reduced peak intensity may be due to the interactions of curcumin and stabilizing agents during the milling procedure [26]. In this case, after the XRPD analysis, such assumption was not supported, as no interactions were identified (*Supplementary material section*). Therefore, obtained lower values of the melting point of curcumin nanocrystals are due to the changes in the particle size and shape compared to the bulk material.

As a supporting evidence, XRPD analysis confirms that curcumin is always present as polymorph 1 in specimens: F_P80, F_P80/SP_4:1, F_P80/SP_2:1 and bulk curcumin (Figures S1-S4, *Supplementary material section*). Neither polymorphs 2 and 3, nor amorphous state of curcumin were not detected, even though they were discussed by Sanphui *et al.* [38]. Stabilizers palmitate and polysorbate 80 (Figures S5 and S6, *Supplementary material section*) do not contribute to patterns of curcumin in F_P80/SP_4:1 and F_P80/SP_2:1. XRPD patterns of here presented curcumin are quite similar to calculated pattern (from single crystal data) reported by Sanphui *et al.* [38] and XRPD pattern reported by Reid *et al.* [39]. Slight change in unite cell parameters between bulk curcumin and reference one [39] could be attributed to synthesis procedure (Table 5). Bulk curcumin is characterized by large crystallites and low strain. Ball milling provoke important crystallite size and strain change comparing to bulk curcumin, especially for F_P80. Only in that case specimen was contaminated with 29% of zirconium oxide originated from the milling medium (Figure S1, *Supplementary material section*). In F_P80/SP_4:1 and F_P80/SP_2:1 crystallite size decrease for about 25% comparing to bulk curcumin and strain increase for about 400% (Table 5)

All reported results indicate that nanonization and processing under presented experimental condiditions did not cause amorphization or change in the polymorph form.

3.4 Short-term physical stability assessment

In order to check the preliminary physical stability of obtained dispersions, size and size distribution of the nanocrystals was followed for 2 weeks. Moreover, each day samples were visually inspected for any precipitation or organoleptic alternations (evident change of color or gen-

Table 4: MTT assay results (concentrations of curcumin (dissolved) and curcumin nanocrystals expressed in μg/ml that induced 50% decrease in the cell survival (IC50)) and calculated selectivity index of curcumin in a solution and curcumin nanocrystals

	Cytotoxicity assessment			Selectivity index	
Sample	**MRC-5**	**Fem-X**	**HeLa**	**Fem-X**	**HeLa**
Curcumin (solution)*	71.17±22.60	70.75±30.89	15.035±0.615	1.01	4.73
F_P80*	40.36±2.86	30.56±11.9	8.81±2.85	1.32	4.58
F_P80/SO_4:1*	40.59±3.17	21.02±0.77	11.36±5.23	1.93	3.57
F_P80/SO_2:1*	34.63±13.65	56.91±33.55	14.46±0.32	0.61	2.39

All data are results of the three independent experiments, each carried out in triplicate.

* Significantly higher anti-proliferative effect towards HeLa, compared to the effect towards Fem-X and MRC-5 cell lines ($p<0.05$)

Selectivity index is calculated by dividing IC50 obtained for the MRC-5 by IC50 obtained for Fem-X and HeLa cells, respectively.

All data are result of the three independent experiments, each carried out in triplicate.

Table 5: Refined unite cell parameters, average crystallite size* and average strain for: F_P80, F_P80/SP_4:1, F_P80/SP_2:1 and bulk curcumin. Unite cell parameters for reference curcumin [39] is also present as well as reliability factors of the WPPF refinement R_{wp}, R_p, R_{exp} and S for F_P80, F_P80/SP_4:1, F_P80/SP_2:1 and bulk curcumin

	F_P80	**F_P80/SP_4:1**	**F_P80/SP_2:1**	**Bulk curcumin**	**Reid *et al.* [39]**
***a* (Å)**	12.701(7)	12.7049(18)	12.7063(18)	12.7021(19)	12.6967
***b* (Å)**	7.223(3)	7.2355(6)	7.2351(6)	7.2361(7)	7.1985
***c* (Å)**	19.875(11)	19.886(3)	19.882(3)	19.881(4)	19.9533
***β* (°)**	95.53(3)	95.475(9)	95.481(8)	95.509(10)	95.124
***α*=γ (°)**	90	90	90	90	90
***V* (Å^3)**	1814.9(17)	1819.7(4)	1819.5(4)	1818.9(5)	1816.393
Average size (nm)	19.1(2)	41.1(2)	37.7(2)	55.06(4)	/
Average strain (%)	0.7(2)	0.25(5)	0.28(7)	0.067(15)	/
R_{wp} (%)	6.02	13.05	11.78	19.87	/
R_p (%)	4.58	8.53	7.75	14.63	/
R_{exp} (%)	5.22	4.11	4.03	3.63	/
S	1.15	3.18	2.92	5.47	/

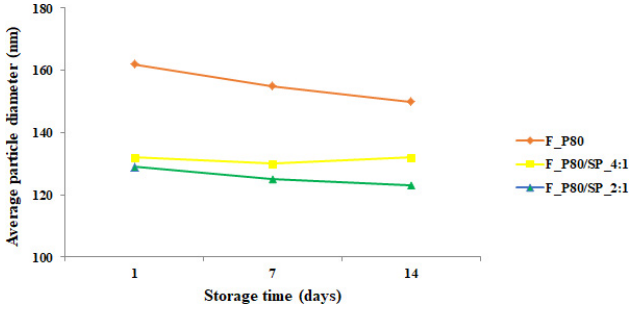

Figure 5: Short-terms physical stability assessment of the investigated curcumin nanocrystal dispersions

eral appearance of the samples). No agglomeration was observed (Figure 5) and no precipitation occurred during this short-term stability check.

3.4.1 *In vitro* dissolution/release study

Targeting potential dermal application, in order to evaluate the dissolution properties of the obtained nanocrystals, selected dispersions were thickened with 1% of xanthan, and the experiment was performed applying Franz diffusion cells.

All samples followed Higuchi's kinetics. Interestingly, comparing the coarse dispersion to the nanocrystal dispersions, completely opposite results were captured. Namely, in the case of nanodispersions, during the 6h of the experiment, F_P80/SP_2:1 reached the highest release, whereas the corresponding coarse dispersion exhibited the lowest release (Figure 6). Obviously, the rank order in the case of nanodispersion formulations correlated to the measured diameter of the nanoparticles. Such finding was somehow expected, as it is well known that decreasing the particle size, saturation solubility and dissolution velocity in-

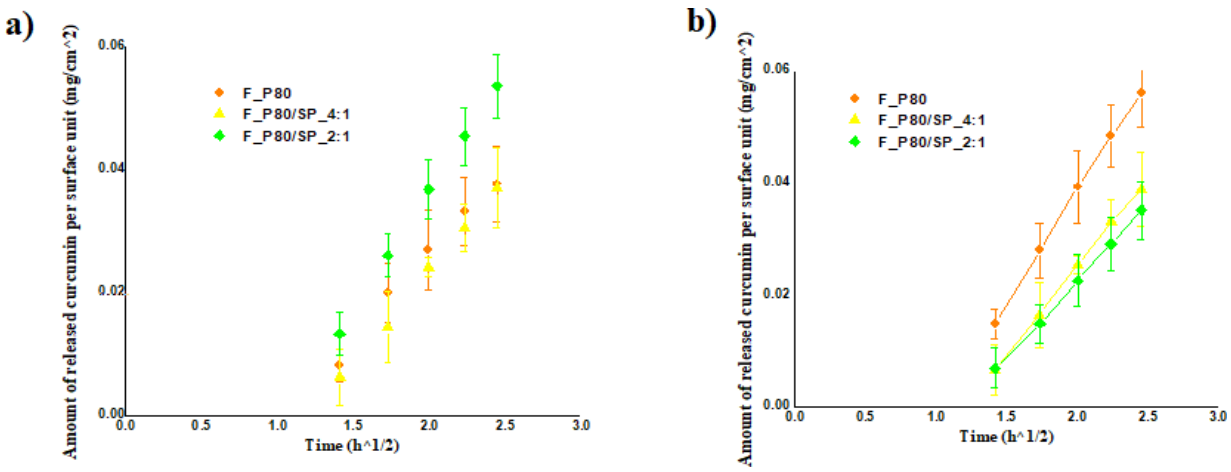

Figure 6: *In vitro* dissolution/release kinetics of the thickened curcumin nanocrystal dispersions (a) and curcumin coarse dispersions (b)

crease due to the bigger contact surface with the solvent and higher dissolution pressure [3, 40]. Such behavior can be explained through the Ostwald– Freundlich equation:

$$log\frac{Cs}{C\infty} = \frac{2\delta V}{2.303RT\rho r} \quad (4)$$

where C_s and C_∞ denote saturation solubility and solubility of the material consisting of large particles (respectively), R is universal gas constant, T absolute temperature, V is molar volume of the material, δ is interfacial tension, ρ represents density of the solid material, and r is the radius. Accordingly, for particles having radius smaller than 1 µm, solubility rises exponentially when radius decreases.

On the other hand, for the coarse dispersions, particle size was not the limiting feature. A reasonable explanation of the obtained rank order of the formulations may be the fact that P80 behaved as a good solubilizer, providing better dissolution rate.

In addition, comparing the total dissolved and released amount of curcumin from the corresponding suspensions, the nanocrystal formulations were significantly superior in each case, highlighting the beneficial effect of the nanodispersed systems.

3.5 Antioxidant activity evaluation

To demonstrate the antioxidant scavenging potential of curcumin nanocrystals, DPPH test was performed. As a parameter of interest, the concentration that inhibits 50% of the free radical in the selected experimental setting was determined (IC50). Also, comparing the results obtained with the bulk curcumin, this test served as a method to check whether any significant change/decrease in the activity occurred during the processing steps in the nanocrystal dispersion preparation.

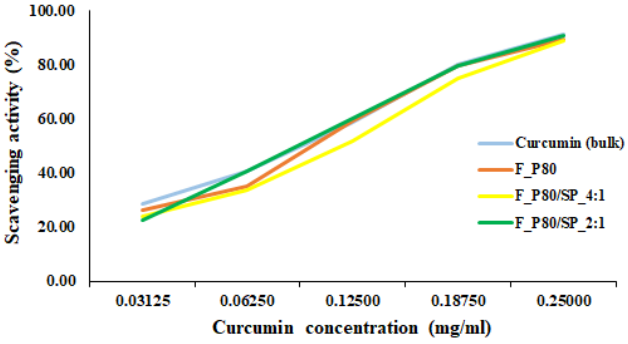

Figure 7: *In vitro* antioxidant activity assessment of the investigated curcumin nanocrystal dispersions: scavenging activity dependence on curcumin concentration

According to the increasing curcumin concentration, there was a visible trend of higher scavenging ability. The IC50 was reached for the curcumin concentration around 0.1 mg/ml. More importantly, all formulations exhibited approximately the same potency (Figure 7), proving that the antioxidant activity was not jeopardized by the preparation steps. However, further experimental work should be performed in more relevant conditions (without organic solvents) where potential prolonged activity of curcumin nanocrystals could be evaluated.

3.6 *In vitro* screening of biological effects

With a view to have an objective insight into the safety and efficacy of the nanocrystal dispersion, cell cytotoxicity assessment was performed applying 3 cell lines: MRC5 for safety screening, and Fem-X and HeLa for obtaining a

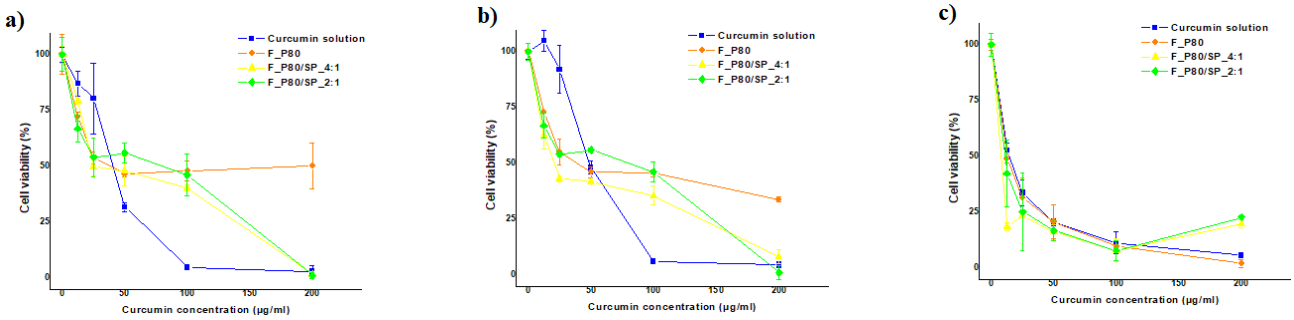

Figure 8: Cell viability assay: a) MRC-5 cell line; b) Fem-X cell line; c) HeLa cell line. Cells were incubated with several concentrations of the investigated curcumin nanocrystal dispersions and curcumin solution. Obtained data show cell viability dependence on the curcumin concentration. Each experiment was repeated three times and the results were presented as the mean value ± SD

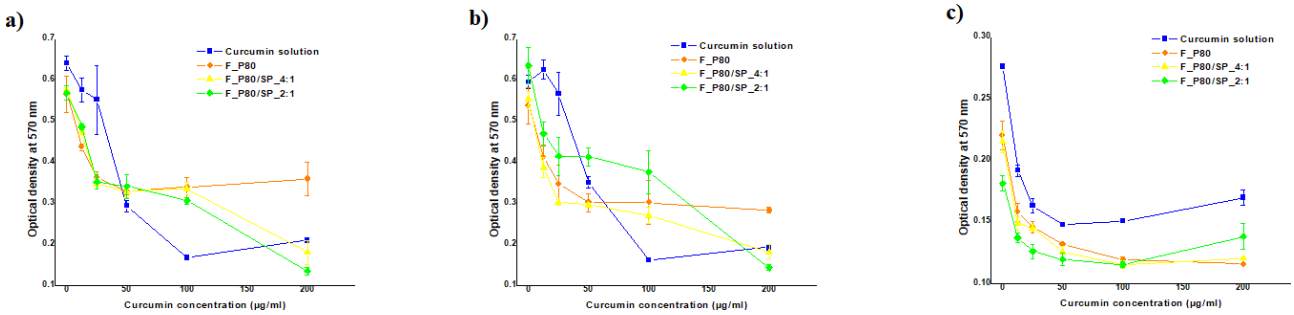

Figure 9: Optical density of the cell cultures after the treatment by the investigated samples: a) MRC-5 cell line; b) Fem-X cell line; c) HeLa cell line. Cells were incubated with several concentrations of the curcumin nanocrystal dispersions and curcumin solution After 48 hours of incubation, MTT reagent was added. Obtained data show optical density of the cell cultures (570 nm) for the selected sample concentrations. Each experiment was repeated three times and the results were presented as the mean value ± SD

clue on efficacy. Having in mind prospective dermal application, efficacy aspects on MRC-5 were recognized as more important.

Regarding MRC-5 and Fem-X, no safety issues were found for the blank samples, whereas HeLa cells were affected even by the blank samples, but in the higher concentrations (*Supplementary material section*). However, based on overall assessment, it can be seen that HeLa cells were generally more susceptible to the cytotoxic effect, as the calculated IC50 values (Table 4) are significantly lower in the case of HeLa compared to other two cell lines. Similar results have already been published with curcumin-loaded nanoemulsions [20]. Moreover, curcumin exhibited an effect to each cell line, but in the nanocrystal form the concentration dependent cell viability decay was less sharp (Figure 8, Figure 9), especially for MRC5 and FemX. Considering selectivity index as a measure of discriminative ability of the formulation to perform cytotoxic effect, it was found that HeLa cells were visibly more affected compared to the Fem-X cells (Table 4). More importantly, even though the tested formulations are nanosuspensions, which is unusual in terms of cytotoxicity assessment, no morphological changes were captured (data not shown) compared to the pure curcumin solution. However, IC50 values in the case of curcumin nanosuspensions are significantly higher. Therefore, we may not exclude some potential mechanical damage, due to particle deposition.

4 Conclusion

Based on the overall assessment, it has been shown that the presented method, mimicking the wet ball milling procedure (but with significantly lower sample amounts), was appropriate for the nanocrystal dispersion preparation for preliminary studies. It is noteworthy that small-scale production units are extremely important in cases when only limited amounts of active pharmaceutical ingredient are available (*e.g.* with newly discovered active compounds). With this regarded, presented approach might represent a good option in preclinical drug evaluation.

It was depicted that the optimal particles in terms of size and size distribution were obtained after 30 minutes of milling, under the speed of 3000 rpm. However, it is noteworthy that the particles' fineness is a function of a particle

shape and the nature of a specific molecule [24]. Selected dispersions stabilized by P80 and its combinations with SP were stable, and curcumin's antioxidant ability was unaltered after the nanonization. Moreover, in cell viability assay, significant anticancer effect of curcumin and curcumin nanocrystals was observed.

The size of obtained particles is comparable to some lipid-based system that have already been developed and investigated for curcumin delivery [23, 41]. Due to significantly lower surfactant concentration, safety profile of nanosuspensions is highly improved compared to other systems with nanostructure, while biological performances remain unaltered. Therefore, the application areas of nanosuspensions are broader.

It should be underlined that many research publications dealt with curcumin nanocrystals in terms of preparation method and physical aspects [26, 28, 30, 42–44]. However, little has been done to evaluate the biological performances of this pleiotropic molecule after the processing, even though its susceptibility to physicochemical degradation is well known. Therefore, a comprehensive approach in the presented work should provide some new insights. Still, further considerations should be taken into account in order to fully characterize these systems.

Acknowledgement: This work was financially supported by the Ministry of Education, Science and Technological Development of the Republic of Serbia (Grant No. 451-03-68/2020-14/200026).

References

[1] Lipinski, C. A. Solubility in water and DMSO: Issues and potential solutions. In *Pharmaceutical profiling in drug discovery for lead selection* (R. Borchardt, E. Kerns, C. Lipinski, D. Thakker, and B. Wang, eds.), AAPS Press, Arlington, TX, 2005, pp. 93–125.

[2] Peltonen, L., and J. Hirvonen. Drug nanocrystals - Versatile option for formulation of poorly soluble materials. *International Journal of Pharmaceutics*, Vol. 537, No. 1-2, 2018, pp. 73–83.

[3] Junghanns, J. U. A., and R. H. Müller. Nanocrystal technology, drug delivery and clinical applications. *International Journal of Nanomedicine*, Vol. 3, No. 3, 2008, pp. 295–309.

[4] Sousa, D., D. Ferreira, J. L. Rodrigues, and L. R. Rodrigues. Nanotechnology in Targeted Drug Delivery and Therapeutics. In *Applications of Targeted Nano Drugs and Delivery Systems*, Elsevier, 2019, pp. 357–409.

[5] Patra, J. K., G. Das, L. F. Fraceto, E. V. R. Campos, M. D. P. Rodriguez-Torres, L. S. Acosta-Torres, et al. Nano based drug delivery systems: Recent developments and future prospects. *Journal of Nanobiotechnology*, Vol. 16, No. 1, 2018, id. 71.

[6] Mu, Q., J. Yu, L. A. McConnachie, J. C. Kraft, Y. Gao, G. K. Gulati, et al. Translation of combination nanodrugs into nanomedicines: Lessons learned and future outlook. *Journal of Drug Targeting*, Vol. 26, No. 5-6, 2018, pp. 435–447.

[7] Aboalnaja, K. O., S. Yaghmoor, T. A. Kumosani, and D. J. McClements. Utilization of nanoemulsions to enhance bioactivity of pharmaceuticals, supplements, and nutraceuticals: Nanoemulsion delivery systems and nanoemulsion excipient systems. *Expert Opinion on Drug Delivery*, Vol. 13, No. 9, 2016, pp. 1327–1336.

[8] Wilhelm, S., A. J. Tavares, Q. Dai, S. Ohta, J. Audet, H. F. Dvorak, et al. Analysis of nanoparticle delivery to tumours. *Nature Reviews. Materials*, Vol. 1, No. 5, 2016, id. 16014.

[9] Clares, B., A. C. Calpena, A. Parra, G. Abrego, H. Alvarado, J. F. Fangueiro, et al. Nanoemulsions (NEs), liposomes (LPs) and solid lipid nanoparticles (SLNs) for retinyl palmitate: Effect on skin permeation. *International Journal of Pharmaceutics*, Vol. 473, No. 1-2, 2014, pp. 591–598.

[10] Ventola, C. L. The nanomedicine revolution: part 1: emerging concepts. *P&T*, Vol. 37, No. 9, 2012, pp. 512–525.

[11] Tuomela, A., J. Hirvonen, and L. Peltonen. Stabilizing agents for drug nanocrystals: Effect on bioavailability. *Pharmaceutics*, Vol. 8, No. 2, 2016, id. 16.

[12] Paradise, J. Regulating nanomedicine at the food and drug administration. *AMAJournal of Ethics*, Vol. 21, No. 4, 2019, pp. E347–E355.

[13] Choi, Y. H., and H. K. Han. Nanomedicines: Current status and future perspectives in aspect of drug delivery and pharmacokinetics. *Journal of Pharmaceutical Investigation*, Vol. 48, No. 1, 2018, pp. 43–60.

[14] Ventola, C. L. Progress in nanomedicine: Approved and investigational nanodrugs. *P&T*, Vol. 42, No. 12, 2017, pp. 742–755.

[15] D'Mello, S. R., C. N. Cruz, M. L. Chen, M. Kapoor, S. L. Lee, and K. M. Tyner. The evolving landscape of drug products containing nanomaterials in the United States. *Nature Nanotechnology*, Vol. 12, No. 6, 2017, pp. 523–529.

[16] Hafner, A., J. Lovrić, G. P. Lakoš, and I. Pepić. Nanotherapeutics in the EU: An overview on current state and future directions. *International Journal of Nanomedicine*, Vol. 9, 2014, pp. 1005–1023.

[17] Colombo, M., S. Staufenbiel, E. Rühl, and R. Bodmeier. In situ determination of the saturation solubility of nanocrystals of poorly soluble drugs for dermal application. *International Journal of Pharmaceutics*, Vol. 521, No. 1-2, 2017, pp. 156–166.

[18] Müller, R. H., S. Gohla, and C. M. Keck. State of the art of nanocrystals—Special features, production, nanotoxicology aspects and intracellular delivery. *European Journal of Pharmaceutics and Biopharmaceutics*, Vol. 78, No. 1, 2011, pp. 1–9.

[19] Ahire, E., S. Thakkar, M. Darshanwad, and M. Misra. Parenteral nanosuspensions: A brief review from solubility enhancement to more novel and specific applications. *Acta Pharmaceutica Sinica. B*, Vol. 8, No. 5, 2018, pp. 733–755.

[20] Nikolic, I., E. Mitsou, A. Damjanovic, V. Papadimitriou, J. Antic-Stankovic, B. Stanojevic, et al. Curcumin-loaded low-energy nanoemulsions: Linking EPR spectroscopy-analysed microstructure and antioxidant potential with in vitro evaluated biological activity. *Journal of Molecular Liquids*, Vol. 301, 2020, id. 112479.

[21] Sharma, R. A., A. J. Gescher, and W. P. Steward. Curcumin: The story so far. *European Journal of Cancer*, Vol. 41, No. 13, 2005, pp. 1955–1968.

[22] Corrias, F., M. Schlich, C. Sinico, R. Pireddu, D. Valenti, A. M. Fadda, et al. Nile red nanosuspensions as investigative model to

study the follicular targeting of drug nanocrystals. *International Journal of Pharmaceutics*, Vol. 524, No. 1-2, 2017, pp. 1–8.

[23] Nikolic, I., D. Jasmin Lunter, D. Randjelovic, A. Zugic, V. Tadic, B. Markovic, et al. Curcumin-loaded low-energy nanoemulsions as a prototype of multifunctional vehicles for different administration routes: Physicochemical and in vitro peculiarities important for dermal application. *International Journal of Pharmaceutics*, Vol. 550, No. 1-2, 2018, pp. 333–346.

[24] Schwarz, J. C., V. Klang, M. Hoppel, D. Mahrhauser, and C. Valenta. Natural microemulsions: Formulation design and skin interaction. *European Journal of Pharmaceutics and Biopharmaceutics*, Vol. 81, No. 3, 2012, pp. 557–562.

[25] Kakran, M., R. Shegokar, N. G. Sahoo, L. A. Shaal, L. Li, and R. H. Müller. Fabrication of quercetin nanocrystals: Comparison of different methods. *European Journal of Pharmaceutics and Biopharmaceutics*, Vol. 80, No. 1, 2012, pp. 113–121.

[26] Hu, L., D. Kong, Q. Hu, N. Gao, and S. Pang. Evaluation of high-performance curcumin nanocrystals for pulmonary drug delivery both in vitro and in vivo. *Nanoscale Research Letters*, Vol. 10, No. 1, 2015, id. 381.

[27] Peltonen, L., and J. Hirvonen. Pharmaceutical nanocrystals by nanomilling: Critical process parameters, particle fracturing and stabilization methods. *Journal of Pharmacy and Pharmacology*, Vol. 62, No. 11, Nov. 2010, pp. 1569–1579.

[28] Rachmawati, H., L. Al Shaal, R. H. Müller, and C. M. Keck. Development of curcumin nanocrystal: Physical aspects. *Journal of Pharmaceutical Sciences*, Vol. 102, No. 1, 2013, pp. 204–214.

[29] Keck, C. M., and R. H. Müller. Drug nanocrystals of poorly soluble drugs produced by high pressure homogenisation. *European Journal of Pharmaceutics and Biopharmaceutics*, Vol. 62, No. 1, 2006, pp. 3–16.

[30] Rachmawati, H., A. Rahma, L. Al Shaal, R. H. Müller, and C. M. Keck. Destabilization mechanism of ionic surfactant on curcumin nanocrystal against electrolytes. *Scientia Pharmaceutica*, Vol. 84, No. 4, 2016, pp. 685–693.

[31] Wang, Y., Y. Zheng, L. Zhang, Q. Wang, and D. Zhang. Stability of nanosuspensions in drug delivery. *Journal of Controlled Release*, Vol. 172, No. 3, 2013, pp. 1126–1141.

[32] Müller, R. H., D. Harden, and C. M. Keck. Development of industrially feasible concentrated 30% and 40% nanoemulsions for intravenous drug delivery. *Drug Development and Industrial Pharmacy*, Vol. 38, No. 4, 2012, pp. 420–430.

[33] Mitrović, J. R., B. Divović, D. E. Knutson, J. B. Đoković, P. J. Vulić, D. V. Randjelović, et al. Nanocrystal dispersion of DK-I-56-1, a poorly soluble pyrazoloquinolinone positive modulator of α6 GABAA receptors: Formulation approach toward improved in vivo performance. *European Journal of Pharmaceutical Sciences*, Vol. 152, 2020, id. 105432.

[34] Willart, J. F., and M. Descamps. Solid state amorphization of pharmaceuticals. *Molecular Pharmaceutics*, Vol. 5, No. 6, Nov.-Dec. 2008, pp. 905–920.

[35] Pawlow, P. The dependency of the melting point on the surface energy of a solid body. *Journal of Physical Chemistry*, Vol. 65, No. 5, 1909, pp. 545–548.

[36] Lu, H. M., P. Y. Li, Z. H. Cao, and X. K. Meng. Size-, shape-, and dimensionality-dependent melting temperatures of nanocrystals. *Journal of Physical Chemistry C*, Vol. 113, No. 18, 2009, pp. 7598–7602.

[37] Guisbiers, G., and L. Buchaillot. Size and shape effects on creep and diffusion at the nanoscale. *Nanotechnology*, Vol. 19, No. 43, 2008, id. 435701.

[38] Sanphui, P., N. R. Goud, U. B. Khandavilli, S. Bhanoth, and A. Nangia. New polymorphs of curcumin. *Chemical Communications*, Vol. 47, No. 17, 2011, pp. 5013–5015.

[39] Reid, J. W., J. A. Kaduk, S. V. Garimella, and S. T. John. Rietveld refinement using synchrotron powder diffraction data for curcumin, C21H20O6, and comparison with density functional theory. *Powder Diffraction*, Vol. 30, No. 1, 2015, pp. 67–75.

[40] Müller, R. H., and K. Peters. Nanosuspensions for the formulation of poorly soluble drugs: I. Preparation by a size-reduction technique. *International Journal of Pharmaceutics*, Vol. 160, No. 2, 1998, pp. 229–237.

[41] Nikolic, I., E. Mitsou, I. Pantelic, D. Randjelovic, B. Markovic, V. Papadimitriou, A. Xenakis, D. J. Lunter, A. Zugic, and S. Savic. Microstructure and biopharmaceutical performances of curcumin-loaded low-energy nanoemulsions containing eucalyptol and pinene: Terpenes' role overcome penetration enhancement effect? *European Journal of Pharmaceutical Sciences*, Vol. 142, 2020, id. 105135.

[42] Bonaccorso, A., M. R. Gigliobianco, R. Pellitteri, D. Santonocito, C. Carbone, P. Di Martino, et al. Optimization of Curcumin Nanocrystals as Promising Strategy for Nose-to-Brain Delivery Application. *Pharmaceutics*, Vol. 12, No. 5, 2020, id. 476.

[43] He, Y., Y. Liang, J. C. W. Mak, Y. Liao, T. Li, R. Yan, et al. Size effect of curcumin nanocrystals on dissolution, airway mucosa penetration, lung tissue distribution and absorption by pulmonary delivery. *Colloids and Surfaces. B, Biointerfaces*, Vol. 186, 2020, id. 110703.

[44] Vidlářová, L., G. B. Romero, J. Hanuš, F. Štěpánek, and R. H. Müller. Nanocrystals for dermal penetration enhancement – Effect of concentration and underlying mechanisms using curcumin as model. *European Journal of Pharmaceutics and Biopharmaceutics*, Vol. 104, 2016, pp. 216–225.

Supplementary Materials

X-ray powder diffraction analysis

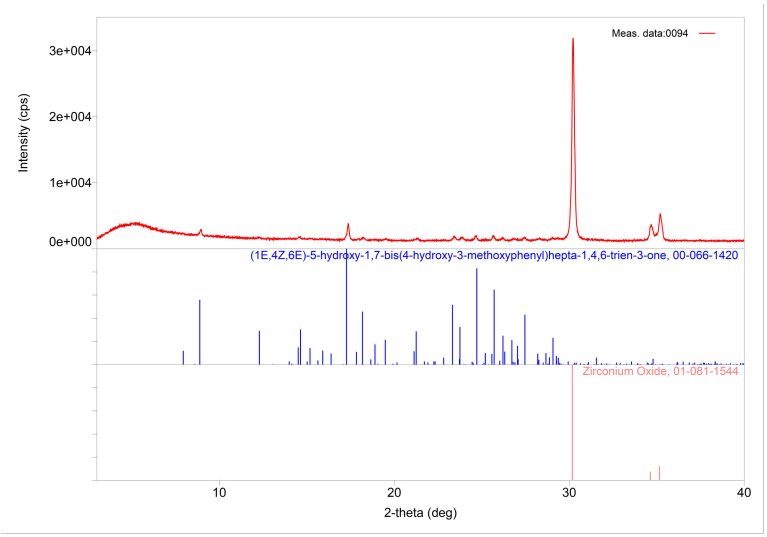

Figure S1: XRPD pattern for F_P80. Reference XRPD patterns for curcumin (card number 00-066-1420; ICDD (PDF-2 Release 2016 RDB)) and zirconium oxide (card number 01-081-1544; ICDD (PDF-2 Release 2016 RDB)) in blue and red are below the experimental pattern. Specimen contains 71(1)% of curcumin and 29(1)% of zirconium oxide.

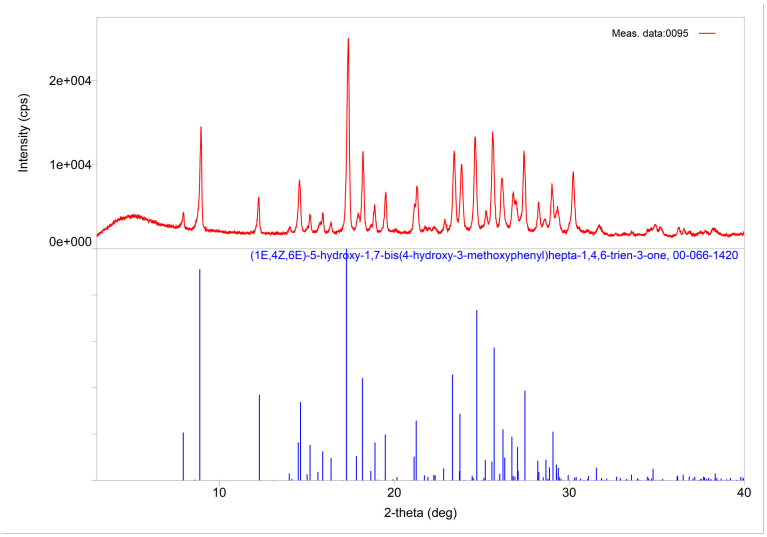

Figure S2: XRPD pattern for F_P80/SP_4:1. Reference XRPD pattern for curcumin (card number 00-066-1420; ICDD (PDF-2 Release 2016 RDB)) in blue is below the experimental pattern.

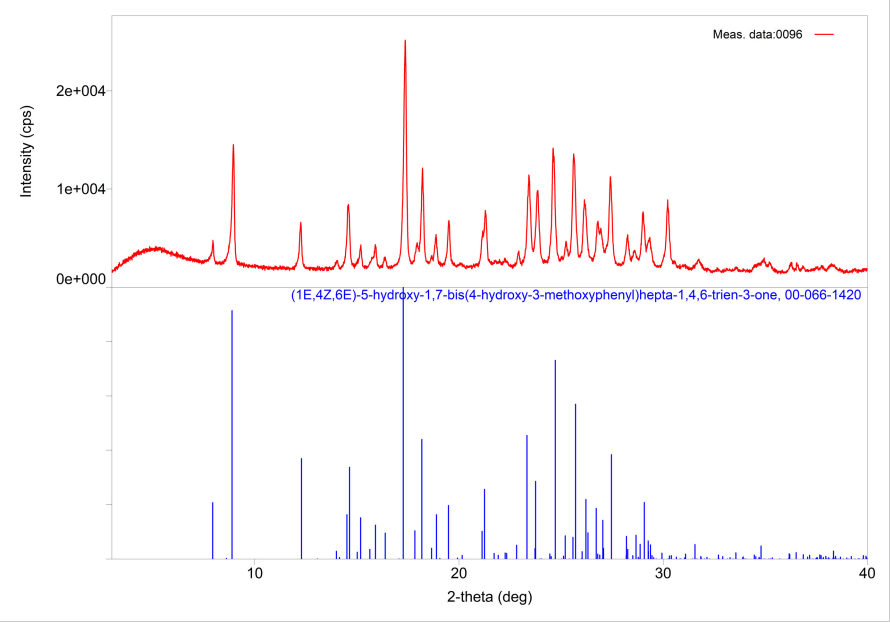

Figure S3: XRPD pattern for F_P80/SP_2:1. Reference XRPD pattern for curcumin (card number 00-066-1420; ICDD (PDF-2 Release 2016 RDB)) in blue is below the experimental pattern.

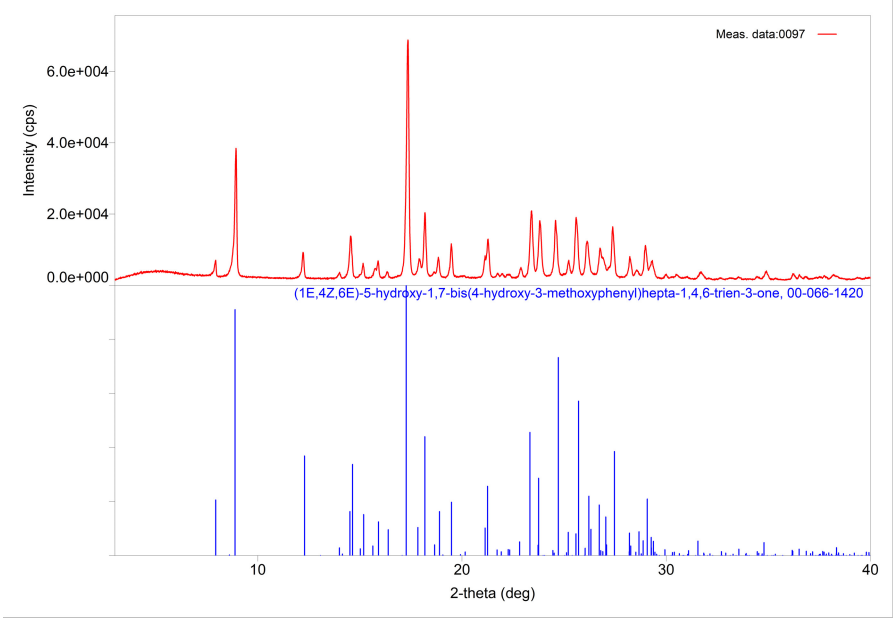

Figure S4: XRPD pattern for bulk curcumin. Reference XRPD pattern for curcumin (card number 00-066-1420; ICDD (PDF-2 Release 2016 RDB)) in blue is below the experimental pattern.

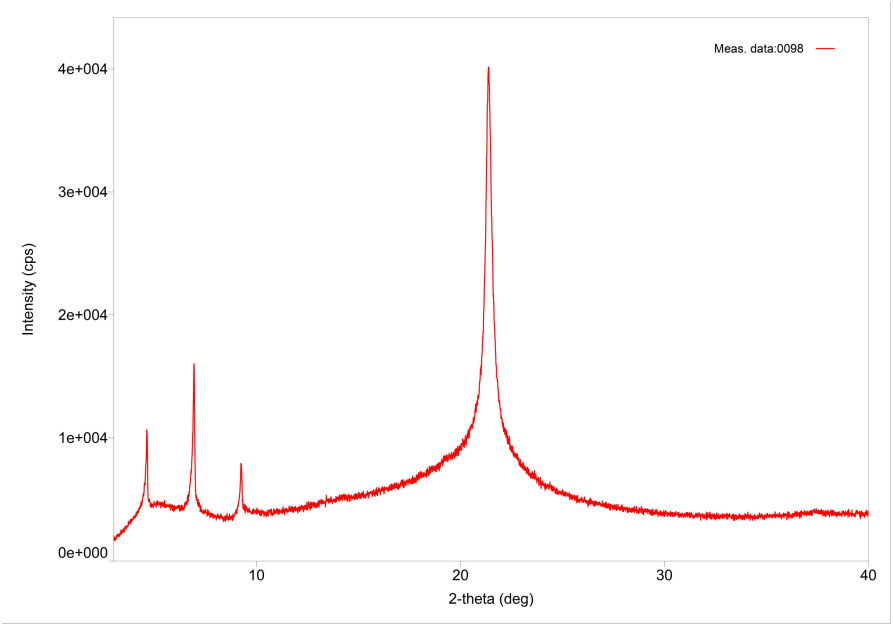

Figure S5: XRPD pattern for sucrose palmitate.

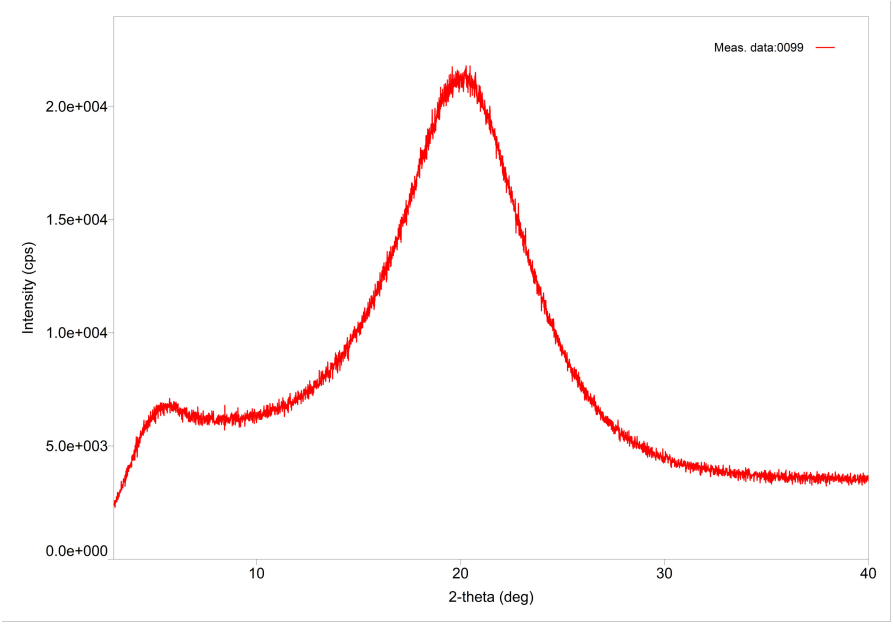

Figure S6: XRPD pattern for polysorbate 80.

In vitro dissolution/release study

In order to be easier for application, selected nanosuspensions and corresponding coarse suspensions were thickened by xanthan gum (1%). The study was performed using *Franz* diffusion cells (*Gauer Glas*, *D-Püttlingen*, Germany). In each cell, 1g of the formulation was deposited. The study was performed in triplicate.

As acceptor medium ethanol 50% *v/v* was used (Nikolic *et al.*, 2018). Each cell receptor chamber was filled with ethanol 50 % *v/v* (chamber volume: 12 mL; effective diffusion area: 2.01 cm^2), preheated to 32°C. Polycarbonate membranes (Nuclepore™, Whatman, Maidstone, United Kingdom; pore dimeter: 0.1 μm), activated in the same ethanol solution during 12-hours period, were carefully placed on top of the receiver compartment, and then the donor and acceptor chamber were fastened. Any existing air bubbles were removed. The donor chamber was filled with 1 g of the samples being investigated, and afterwards covered with silicone film (ParafilmTM, USA) to prevent evaporation and loss of the formulation during sampling. Cells were placed in the water bath where the temperature of 32°C was maintained through the whole experiment. Acceptor phase was under continuous magnetic stirring at 500 rpm. Release study was performed for 6 hours. Aliquots of 0.6 μL of the acceptor phase were withdrawn at 6 time points (0.5 h, 1h, 2h, 3h, 4h and 6h), and then replaced with the same volume of fresh and thermostated ethanol solution. LC-MS/MS technique was used for determination of curcumin content. Aiming to find the model that best describes the drug liberation profile from investigated samples, cumulative amounts of curcumin per unit area were evaluated through several kinetic models.

LC-MS/MS analysis

Determination of curcumin content during the release/dissolution study was performed by liquid chromatography coupled with mass spectrometry (LC-MS/MS) technique Liquid chromatographic system with Accela autosampler and the pump (Thermo Fisher Scientific, San Jose, CA) was applied, and analysis was conducted under established separation conditions. Xterra® MS C18 column (3,5 μm 2,1×150 mm; Waters Corporation, Ireland) was used for the separation, at 25°C. A mobile phase consisting of acetonitrile and 0.1% formic acid aqueous solution (70:30 v/v) was used for isocratic elution, at flow rate of 0.3 mL/min, and run time of 5 minutes. Mass analyses were conducted on TSQ Quantum Access MAX triple quadrupole mass analyzer equipped with electrospray ionization (ESI) source and high-purity nitrogen as nebulizing gas. Selected reaction monitoring (SRM) for data collecting was in positive mode, and ESI source and mass spectrometry parameters were at following values: spray voltage - 5000 V; vaporizer temperature - 400°C; sheath gas pressure - 30 units; ion sweep gas pressure - 0 units; auxiliary gas - 15 units; ion transfer capillary temperature - 250°C; capillary offset - 35 units; skimmer offset - 0 units; m/z 369,2→ 177,0; collision energy – 22 V; peak width - 0.7; scan time - 200 ms. The data were processed through Xcalibur software v 2.1.0.1139 (Thermo Fisher Scientific).

In vitro screening of biological effects

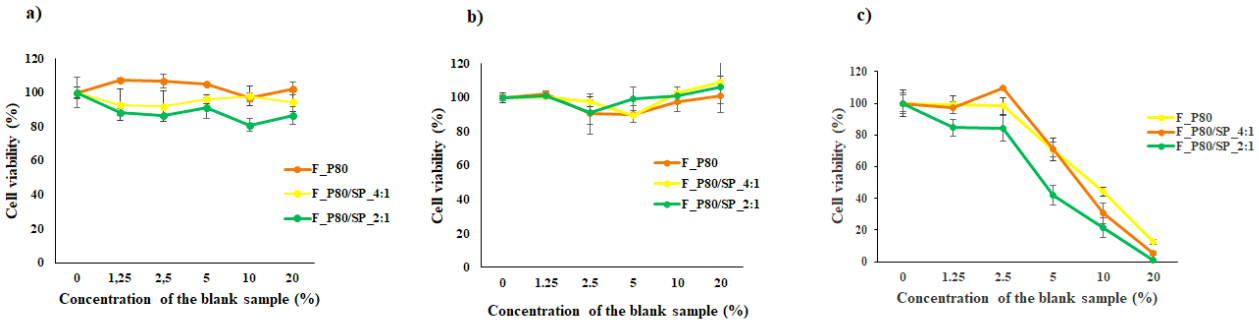

Figure S7: Cell viability assay: a)MRC-5 cell line; b) Fem-X cell line; c) HeLa cell line. Cells were incubated with several concentrations of the corresponding blank samples. Obtained data show cell viability dependence on the blank sample concentration. Each experiment was repeated three times and the results were presented as the mean value ± SD.